Manipulating the Orientations of the Electric and Magnetic Dipoles Induced in Silicon Nanoparticles for Multicolor Display

Jin Xiang, Juntao Li, Zhenpeng Zhou, Shuai Jiang, Jingdong Chen, Qiaofeng Dai, ShaoLong Tie, Sheng Lan,* and Xuehua Wang*

Artificial control of colors based on plasmonic and dielectric nanostructures is not only interesting for fundamental research, but also important for practical applications. Apart from spatial resolution, chromaticity, angular independence, and dynamical color-tuning have emerged as the most desirable functions for structural color. Here, it is shown theoretically that the orientations of the electric or magnetic dipoles induced in a silicon nanoparticle can be manipulated by using an evanescent wave excited by *s*- or *p*-polarized light, and it is experimentally demonstrated that the scattering light color can be controlled by simply varying the polarization of the illumination light. It is revealed that the excitation of a silicon nanoparticle using an evanescent wave is equivalent to that of using both the incident and reflected light, enabling the manipulation of the scattering light color by controlling the orientations of the electric and magnetic dipoles. In addition, an enhanced scattering light intensity and a completely dark background are achieved by using evanescent wave excitation. More importantly, a color-tuning display with a spatial resolution close to the optical diffraction limit, and a good chromaticity on an array of silicon nanopillars fabricated on a silica substrate is demonstrated, which are compatible with the current fabrication technology of silicon chips.

1. Introduction

Artificial control of colors can be realized by employing either plasmonic or dielectric nanostructures and it has attracted tremendous interest in recent years owing to its potential applications in printing, display, and filters etc. The indexes commonly used for evaluating the structural colors include spatial resolution, chromaticity, angular independence, and tunable ability.[1]

As compared with traditional dyes/pigments or semiconductor quantum dots, which can create vivid and angle-independent colors, the most important advantage of artificial nanostructures is the significantly improved spatial resolution which can be close to the optical diffraction limit.

Recently, the surface plasmon resonances (SPRs) in metallic nanoparticles/nanostructures have been employed to downscale the spatial resolution to the optical diffraction limit and pixel size as small as ≈250 nm has been successfully demonstrated.[2] The small dimensions of plasmonic nanostructures also offer the possibility of creating various colors by using the combination of different nanostructures.[1–18] In general, the structural colors created by plasmonic nanostructures show angular independence which is important for color display.[8] Owing to the large ohmic loss of metals in the visible light spectrum, however, the reflection or transmission of periodically arranged metallic nanoparticles/nanostructures usually exhibits a bandwidth larger than 150 nm, leading to a low chromaticity.[19]

As compared with their plasmonic counterparts, dielectric nanoparticles/nanostructures with large refractive index and low ohmic loss,[20] such as silicon (Si) nanoparticles, also exhibit structural colors because of the existence of distinct electric and magnetic dipole (ED and MD) resonances in the visible light

J. Xiang, S. Jiang, J. Chen, Prof. Q. Dai, Prof. S. Lan
Guangdong Provincial Key Laboratory of Nanophotonic Functional Materials and Devices
School of Information and Optoelectronic Science and Engineering
South China Normal University
Guangzhou 510006, China
E-mail: slan@scnu.edu.cn

Prof. J. Li, Z. Zhou, Prof. X. Wang
State Key Laboratory of Optoelectronic Materials and Technologies
School of Physics
Sun Yat-Sen University
Guangzhou 510275, China
E-mail: wangxueh@mail.sysu.edu.cn

Prof. S. Tie
School of Chemistry and Environment
South China Normal University
Guangzhou 510006, China

The ORCID identification number(s) for the author(s) of this article can be found under https://doi.org/10.1002/lpor.201800032

**ADVANCED
SCIENCE NEWS**

www.advancedsciencenews.com

LASER
& PHOTONICS
REVIEWS

www.lpr-journal.org

spectrum.[21–26] The Mie resonances in such dielectric nanoparticles possess line widths comparable to those of the SPRs of plasmonic nanoparticles/nanostructures.[27] However, the ED and MD resonances of a Si nanoparticle are simultaneously excited in both bright- and dark-field illuminations, leading to broadband scattering light.[28,29] Although the reduction in either the ED or the MD resonance can be achieved by using an oblique incidence,[30] the selective excitation of the ED or MD resonance remains a significant challenge. Recently, a coherent spectroscopy based on the standing wave formed by two counterpropagating light beams was proposed to selectively excite the ED or MD resonance of a plasmonic metamaterial by placing it at the nodes of magnetic or electric field of the standing wave.[32,33] In addition to the bandwidth, the scattering light intensity of single Si nanoparticles need to be enhanced when only a single Si nanoparticle is used in a pixel to achieve a high spatial resolution.

Color display based on regularly arranged silicon (Si),[28,31,34–39] germanium (Ge)[40] and titanium dioxide (TiO_2)[29] nanopillars (NPs) has been successfully demonstrated. For Si-based arrays, a thin film of amorphous Si deposited on a silica substrate was used to fabricate Si NPs.[26] Since the imaginary part of amorphous Si is much larger than that of crystal Si, the chromaticity of the arrays is not satisfied because of the broadened electromagnetic resonances. Very recently, Si nanostructures that exhibit localized magnetic and electric dipole resonances were fabricated on a silicon substrate coated with a Si_3N_4 index matching layer to mimic Si nanostructures in free space.[34] This novel design broadens the color gamut while retaining print resolution. For TiO_2-based arrays, the Fano resonances generated by periodically arranged TiO_2 NPs are employed to significantly enhance the reflectance because the reflection of a single TiO_2 NP is too weak.[41] In this way, the chromaticity of the arrays is improved by the narrower Fano resonances.[19,29] Unfortunately, the improvement in chromaticity is achieved by sacrificing the spatial resolution, which is far from the optical diffraction limit.

In practice, tunable ability is also very important in color control, especially in display. So far, color-tuning has been realized by using liquid crystals on plasmonic surface,[42] electrochromic polymers,[6] mechanical actuation on plasmonic and silicon structures,[43] and polarization control of asymmetric nanoparticles.[44] From the viewpoint of practical application, however, the achievement of a wide color-tuning range by using a simple and convenient method is highly desirable for multicolor display.

A survey of the current literature reveals that the artificial control of colors is mainly achieved by using either plasmonic or dielectric nanostructures. Beneficial from the current fabrication technology, the spatial resolution for both kinds of nanostructures can exceed the optical diffraction limit (250–300 nm).[3,8,18,40,45,46] Unfortunately, the linewidth of the resonances, which influences the chromaticity of the structural color, is generally very large due to the dissipative loss of plasmonic nanostructures or the simultaneous appearance of the ED and MD resonances in dielectric nanostructures. In some cases, significantly reduced linewidth is achieved by using a periodic nanostructure rather than a single nanoparticle in a pixel, scarifying the spatial resolution.[5,19,29] In addition, dynamical control of colors is realized only in rare cases.[5,40,46] Moreover, reflective or dark-field illumination is generally employed in color display,

leading to an unsatisfied contrast because of the background noise.[3,8,18,19,29,40,45,46]

In this article, we propose a new strategy for realizing color-tuning display with high spatial resolution and good chromaticity. We employ an evanescent wave, which offers us the opportunity of manipulating the orientations and phases of the induced EDs and MDs, to excite Si nanoparticles. We reveal that the excitation of a Si nanoparticle by using the evanescent wave is equivalent to the simultaneous excitation of the Si nanoparticle by using both the incident and reflected light, leading to enhanced scattering light and completely dark background. We show theoretically and demonstrate experimentally that the orientations of the ED and MD induced in a Si nanoparticle can be manipulated by using the evanescent wave excited by *s*- or *p*-polarized light, producing vivid structural colors with good chromaticity. By using an array of regularly arranged Si NPs, we demonstrate color-tuning display with a spatial resolution of ≈800 nm by simply varying the polarization of the illumination light.

In the dipole approximation, the scattering properties of a Si nanosphere (NS) are determined by the strength and orientation of the ED and MD induced in the Si NS. In the case of normal incidence, the orientations of the ED and MD are determined by the electric and magnetic fields of the incident wave (see Supplementary Figure S1) and one can observe both the ED and MD resonances in the forward scattering spectrum of the Si NS because the induced ED and MD are perpendicular to the direction of observation.[23–25,30,47] Therefore, the scattering light color of a Si NS is basically determined by its size. In principle, the scattering properties of the Si NS can be modified by varying either the surrounding environment or the illumination configuration.[30] It has been shown that both the forward and backward scattering spectra of a Si NS can be changed by using a metal film.[48] Moreover, it has been demonstrated that optical pulling force acting on a nanoparticle can be generated by using a single Bessel beam or two interfering plane waves which modify the forward and backward scattering properties of the nanoparticle.[49,50] Therefore, controlling the scattering properties of Si nanoparticles by varying the parameters of the incident wave is not only interesting for fundamental research but also desirable for practical application. For example, the physical properties of an array of Si NSs are determined by the spatial orientations of the EDs and MDs induced in the constituent Si NSs. More interestingly, the coupling between Si NSs is also governed by the spatial orientation of the induced EDs and MDs, rendering intriguing transmission or reflection properties of the array which are useful for the construction of functional devices.[51] Since a dipole exhibits a doughnut-shaped radiation pattern, it appears bright in the direction perpendicular to the dipole but becomes almost "invisible" (dark) in the direction parallel to the dipole. This unique feature offers us the opportunity to control the radiation intensity of a dipole in a certain direction by simply varying the orientation of the dipole.

2. Methods

2.1. Experimental Details

We employed femtosecond (fs) laser ablation to fabricate Si NSs with diameters ranging from 150–250 nm. In experiments,

**ADVANCED
SCIENCE NEWS**

www.advancedsciencenews.com

LASER
&PHOTONICS
REVIEWS

www.lpr-journal.org

800 nm fs laser light delivered by a fs amplifier (Legend Elite, Coherent) with pulse duration of 90 fs and repetition rate of 1 kHz was focused on the surface of a crystalline-silicon (c-Si) wafer, which was immersed in deionized water, by using a lens with a focal length of 150 mm. Once the ablation was completed, the aqueous solution containing Si NSs was centrifuged with a speed of 12 000 rpm to separate Si NSs with diameters of 150–250 nm from small Si nanoparticles.

For the fabrication of Si NPs on a silica substrate, 220-nm-thick c-Si film was firstly transferred to a silica substrate by adhesive wafer bonding. Then, a 180-nm-thick electron-beam photoresist (ZEP520A) was spin-coated on the surface of c-Si film and baked at 180 °C for 10 minutes. After that, a 50-nm-thick aluminium (Al) layer was deposited by thermal evaporation to avoid static charging during electron-beam lithography. The pattern was exposed by an electron beam writer (Vistec EBPG-5000plusES, Raith) at an acceleration voltage of 100 KeV. The Al layer was removed by using tetramethylammonium hydroxide and the photoresist was developed by using xylene. The pattern transfer was carried out by using inductively coupled plasma (ICP) (Oxford Instruments) in HBr gas. Finally, the pattern resist was removed by using O_2 plasma etching.

The morphologies of both Si NSs and NPs were examined by scanning electron microscope (SEM) (Ultra55, Zeiss) and transmission electron microscope (TEM) (JEM-2100HR, JEOL) observations. Meanwhile, the scattering properties of Si nanoparticles were characterized by using an inverted microscope (Axio Observer A1, Zeiss) equipped with a spectrometer (SR-500i-B1, Andor) and a charge coupled device (DU970N, Andor).

2.2. Numerical Simulation and Analytical Model

The scattering spectra of Si NSs and NPs were either analytically calculated based on Mie theory or numerically simulated by using the finite-difference time-domain (FDTD) technique. The multipolar contributions to the total scattering of the Si NSs are calculated analytically while the corresponding results of the Si NPs are evaluated numerically based on the decomposition utilizing spherical harmonics. The permittivity of Si was fitted from experimental data.[52] In the FDTD simulation, we employed a total-field/scattered-field source to evaluate the scattering efficiency of Si NSs and NPs. A uniform mesh size with the smallest one of 1 nm was used to obtain converged simulation results and perfectly matched layer boundary condition was employed to terminate the finite simulation region.

The phase difference between the incident and reflected light can be derived based on the Snell equation. The reflectivities of p- and s-polarized light, from which the phase difference can be obtained, are given as follows:

$$r_s = \frac{\cos\varphi - i\sqrt{\sin^2\varphi - n^2}}{\cos\varphi + i\sqrt{\sin^2\varphi - n^2}}, \quad r_p = \frac{n^2\cos\varphi - i\sqrt{\sin^2\varphi - n^2}}{n^2\cos\varphi + i\sqrt{\sin^2\varphi - n^2}} \quad (1)$$

where $n = n_2/n_1$. In our case, n_1 and n_2 are the refractive indices of glass/silica and air, φ is the angle between the incident light and the surface normal (see Supplementary Figure S2).

In the case of total internal reflection, the electric and magnetic fields of the evanescent wave for s-polarized light can be derived as follows:

$$\mathbf{E}'_s = \mathbf{y}E_0'e^{-\beta z}e^{i(k_{2x}x - \omega t)}$$

$$\mathbf{H}'_s = \frac{1}{\mu\omega}E_0'e^{-\beta z}e^{i(k_{2x}x - \omega t)}(-i\beta\mathbf{x} + k_{2x}\mathbf{z}) \quad (2)$$

For p-polarized light, the electric and magnetic fields of the evanescent wave can be expressed as follows:

$$\mathbf{E}'_p = E_0'e^{-\beta z}e^{i(k_{2x}x - \omega t)}\left(-i\frac{\beta}{k_0}\mathbf{x} + \frac{k_{2x}}{k_0}\mathbf{z}\right)$$

$$\mathbf{H}'_p = \mathbf{y}E_0'\sqrt{\varepsilon_0/\mu_0}e^{-\beta z}e^{i(k_{2x}x - \omega t)} \quad (3)$$

Here, $\beta = k_1\sqrt{\sin^2\varphi - n^2}$, k_1 and k_2 are the wave vectors of the incident and transmitted light, ω is angular frequency of the incident light, $\mathbf{x}$, $\mathbf{y}$ and $\mathbf{z}$ are direction vectors of x, y, and z, respectively (see Supplementary Section 2 for details).

3. Results and Discussion

Figure 1a shows the schematic of exciting a Si NS with an evanescent wave and detecting the scattering light in the forward direction. The Si NS is placed on a glass slide which is attached on a prism by Si oil. The evanescent wave, which possesses enhanced fields on the surface of the glass slide (see Supplementary Figure S3), is generated in a total internal reflection configuration. In this case, the excitation of the Si NS by using the evanescent wave is equivalent to that by using two interfering waves, namely the incident and reflected light, as demonstrated in the following. The orientations of the ED and MD excited in the Si NS depend strongly on the polarization of the incident light, as shown in Figure 1b and c. For p-polarized light, the horizontal components of the electric fields of the incident and reflected light are cancelled out while the vertical components of the electric fields and the horizontally-aligned magnetic fields are superimposed, as shown in Figure 1b. Consequently, a horizontally-oriented MD, which appears as bright in the direction of observation (i.e., the z direction), and a vertically-oriented ED, which appears as dark, are induced in the Si NS, as shown in Figure 1a. Thus, only the MD resonance is observed in the forward scattering spectrum. The situation is reversed for s-polarized light, as shown in Figure 1a and c. Since the scattering light is determined by the coherent interaction between the ED and MD induced in the Si NS, scattering light with different colors can be generated by manipulating the orientations of the ED and MD by varying the polarization of the incident light, as schematically shown in the insets of Figure 1a.

Basically, the scattering cross section of a Si NS illuminated by a single plane wave can be calculated based on Mie theory and the differential scattering intensity can be expressed as follows:[43]

$$\left[\frac{dQ}{d\Omega}(\varphi)\right]_{s,p} = \frac{k^4}{16\pi^2}\left|\alpha_{es,mp} + \alpha_{ms,ep}\cos\varphi\right|^2 \quad (4)$$
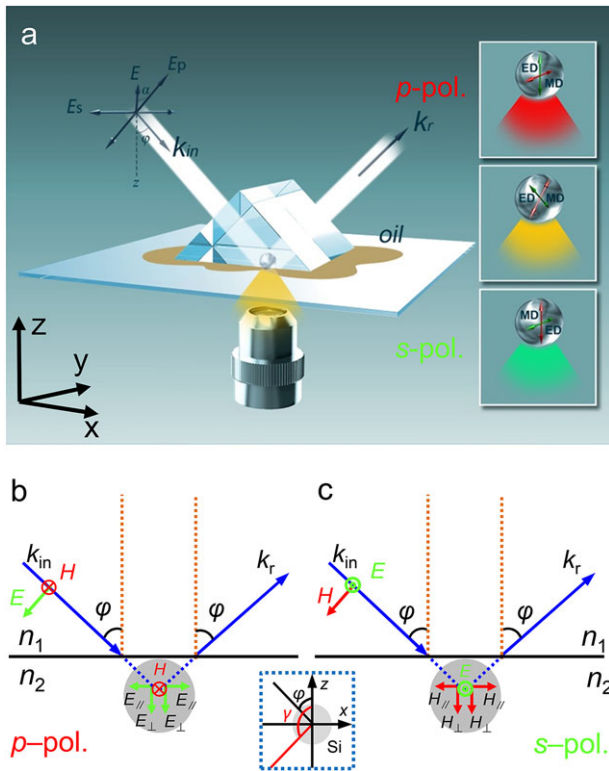
Figure 1. Manipulating the orientations of the ED and MD induced in a Si NS with the evanescent wave excited by p- and s-polarized light. a) Schematic showing the experimental setup used to excite a Si NS with the evanescent wave generated in a total internal reflection configuration and to detect the scattering light of the Si NS in the forward direction. b,c) Schematic showing the excitation of a Si NS by using the evanescent wave which is equivalent to that by using the incident and reflected light. The combined electric and magnetic fields of the incident and reflected light which determine the orientations of the ED and MD induced in the Si NS by p- and s-polarized light are illustrated. Here, φ is the angle between the incident light and the surface normal while γ is the angle between the extension line of the reflected light and the surface normal.

where $\alpha_e = \frac{6\pi a_1 i}{k^3}$, $\alpha_m = \frac{6\pi b_1 i}{k^3}$ with a_1 and b_1 the first-order Mie coefficients in the expansion. Here, the subscripts s and p denote the polarizabilities induced by s- and p-polarized light, respectively. If the Si NS is illuminated by two interfering waves as that in the evanescent wave excitation, the differential scattering intensity can be derived as follows:

$$\left[\frac{dQ}{d\Omega}(\varphi)\right]_{s,p} =$$

$$\frac{k^4}{16\pi^2}\left|\alpha_{es,mp} + \alpha_{es,mp}e^{i\delta_{s,p}} + \alpha_{ms,ep}\cos\varphi + \alpha_{ms,ep}e^{i\delta_{s,p}}\cos\gamma\right|^2 \quad (5)$$

Here, φ is the angle between the incident light and the normal of the glass slide while γ is the angle between the extension line of the reflected light and the normal of the glass slide, δ is the phase difference between the incident and reflected light. It is apparent that $\varphi + \gamma = \pi$ and $\delta = 0$ at the critical angle for total

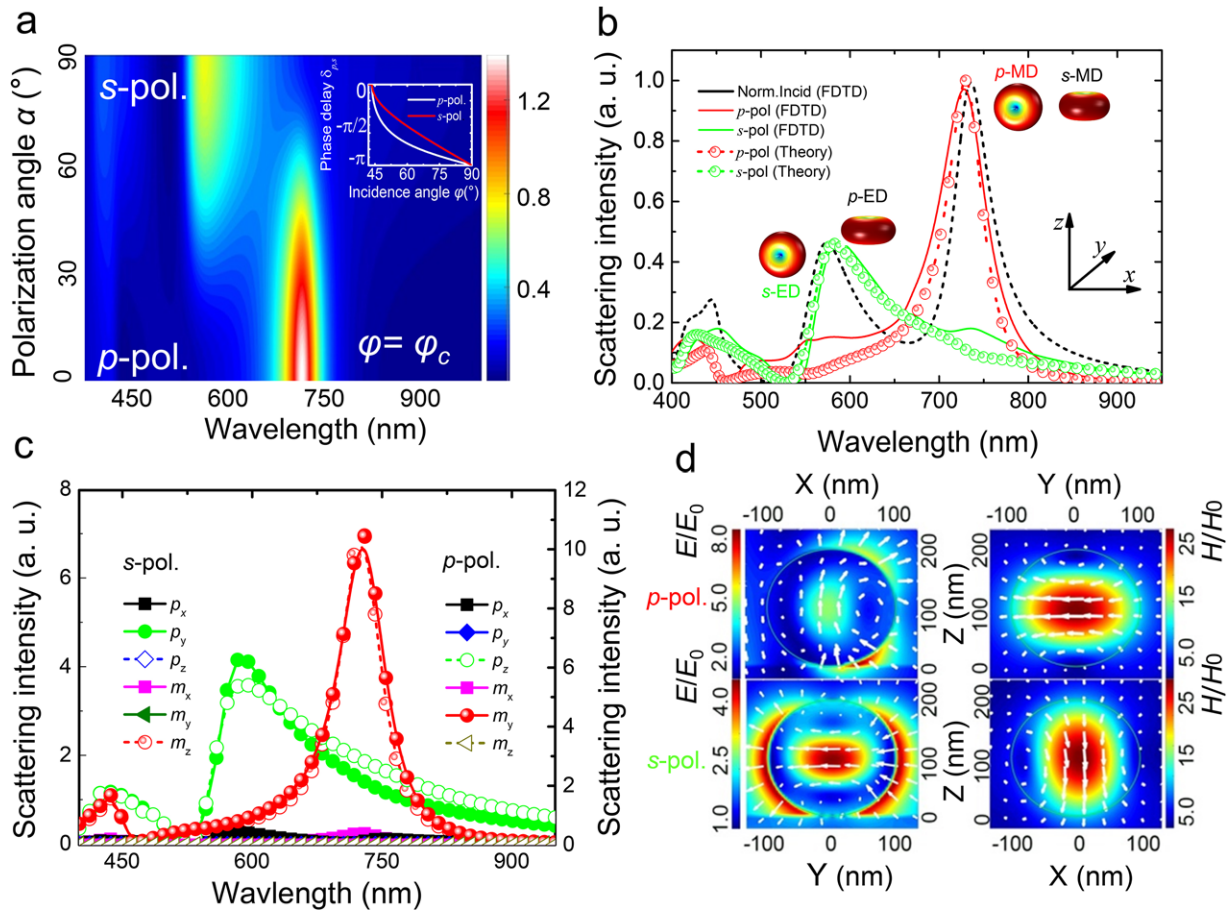internal reflection. Therefore, Equation (5) can be reduced to be

$$\frac{dQ}{d\Omega}(\varphi)_s + \frac{dQ}{d\Omega}(\gamma)_s = \frac{k^4}{4\pi^2}|\alpha_e|^2 \quad (6)$$

$$\frac{dQ}{d\Omega}(\varphi)_p + \frac{dQ}{d\Omega}(\gamma)_p = \frac{k^4}{4\pi^2}|\alpha_m|^2 \quad (7)$$

Equation (6) indicates that only the ED or MD resonance of the Si NS will appear in the forward scattering spectrum when the Si NS is excited by using s- or p-polarized light, implying that the ED or MD resonance of the Si NS can be independently excited. In general, the scattering light of a Si NS with moderate size appears as white because the ED and MD resonances are simultaneously excited. The selective excitation of the ED or MD resonance will make the scattering light green or red (see the insets of Figure 1). For s-polarized light, the MD induced in the Si NS orients vertically along the axis of the objective lens and does not contribute to the forward scattering. The scattering spectrum is dominated by the horizontally-oriented ED which is perpendicular to the axis of the objective lens. For p-polarized light, only the horizontally-oriented MD contributes to the scattering in the forward direction. By changing the polarization angle of the incident light, both the ED and MD resonances are partly excited with different ratios, leading to scattering light with different colors. In this way, one can realize multicolor display by simply controlling the polarization angle of the incident light.

In **Figure 2**a, we show the evolution of the forward scattering spectrum with increasing polarization angle (α) calculated for a Si NS with a diameter (d) of 187 nm. Here, polarization angles of $\alpha = 0°$ and $90°$ correspond to p- and s-polarized light, respectively. It can be seen that only the MD resonance at ≈730 nm is observed when the Si NS is illuminated with p-polarized light. With increasing polarization angle, the intensity of the MD resonance decreases while that of the ED resonance increases gradually. For s-polarized light, the MD resonance disappears completely and only the ED resonance at ≈570 nm is observed in the forward scattering spectrum. The phase difference between the incident and reflected light for p- and s-polarized light is shown in the inset of Figure 2a. It can be seen that the incident and reflected beams are in phase at the critical angle for total internal reflection and this relationship is independent of the polarization of the incident light (see Methods for the details).

In Figure 2b, we show the forward scattering spectra calculated for a Si NS with $d = 187$ nm excited by using s- and p-polarized light based on Equation (6) and (7). The forward scattering spectrum of the Si NS excited by a plane wave under normal incidence is also provided for reference. It can be seen that only the ED or MD resonance is observed when the Si NS is excited by using s- or p-polarized light. In order to validate the theoretical analysis, we also simulated the forward scattering spectra of the Si NS excited by using s- and p-polarized light based on the FDTD technique, as shown in Figure 2b. Although the calculated spectra were obtained for a Si NS suspended in air while the simulated ones were obtained for a Si NS placed on a glass substrate, a good agreement between them is observed except a slight broadening of the ED and MD resonances found in the simulation results. The influence of a substrate on the ED and MD resonances of

ADVANCED
SCIENCE NEWS
www.advancedsciencenews.com

LASER
& PHOTONICS
REVIEWS

www.lpr-journal.org

Figure 2. Selective excitation of the ED or MD resonance of a Si NS. a) Evolution of forward scattering spectrum with increasing polarization angle calculated for a Si NS with $d = 187$ nm. The dependence of the phase difference between the incident and reflected light on the incidence angle calculated for p- and s-polarized light is shown in the inset. b) Normalized forward scattering spectra calculated and simulated for a Si NS with $d = 187$ nm, which are excited by using s- and p-polarized light at the critical angle (43.5°), by using Mie theory and the FDTD method. The normalized forward scattering spectrum of the same Si NS excited by using a plane wave under normal incidence is also provided for comparison. The radiation patterns of the ED and MD induced by s- and p-polarized light are presented as insets. c) Decomposition of the total scattering spectra simulated for a Si NS with $d = 187$ nm, which are excited by using s- and p-polarized light at the critical angle (43.5°), into the contributions of EDs and MDs oriented in different directions. d) Electric and magnetic field distributions in the Si NS calculated for p- (upper part) and s-polarized light (lower part).

a dielectric nanoparticle has been systematically investigated previously[53] and the slight broadening observed here implies that the existence of glass/silica substrates with a low refractive index (≈1.45) has negligible influence on the structural color of Si nanoparticles (see Supplementary Figure S4).

In order to confirm that the orientations of the MD and ED induced in a Si NS can be manipulated by using the evanescent wave excited by p- and s-polarized light, we decomposed the total scattering spectra of a Si NS with $d = 187$ nm obtained for p- and s-polarized light into the contributions of MDs and EDs oriented in different directions (i.e., p_x, p_y, p_z, m_x, m_y, and m_z) by using multipole expansion,[54] as shown in Figure 2c. In this case, the ED and MD induced in the Si NS can be calculated based on the electric field $\mathbf{E}(\mathbf{r})$, i.e., $\mathbf{p} = \int \mathbf{P}d\mathbf{r}$, $\mathbf{m} = \int \mathbf{r} \times \mathbf{P}d\mathbf{r}$, $\mathbf{P} = \varepsilon_0(\varepsilon_p - \varepsilon_d)\mathbf{E}$. Here, ε_0, ε_p, and ε_d are the permeabilities of vacuum, nanoparticle (Si in our case) and environment (air in our case). Different from the Si NS excited by a plane wave (see Supplementary Figure S5), it can be seen clearly that the total scattering of the Si

NS excited by p-polarized light arises from m_y and p_z while that excited by s-polarized originates from p_y and m_z. It implies that one can only observe the radiation of m_y for p-polarized light and the radiation of p_y for s-polarized light in the z direction, as we did in the experiments.

The electric and magnetic field distributions on the XZ and YZ planes calculated for s- and p-polarized light are shown in Figure 2d. For s-polarized light, it can be seen that the MD is made oriented vertically while the ED remains oriented horizontally. As a result, only the radiation of the ED is detected in the forward direction (i.e., the z direction). The situation is reversed when p-polarized light is employed, verifying the orientations of the ED and MD induced in the Si NS shown Figure 2c.

In **Figure 3**a, we show the evolution of forward scattering spectrum with increasing polarization angle calculated for a Si NS with $d = 160$ nm. The experimental results performed for a Si NS with the similar size are shown in Figure 3b. Very good agreement is observed between the calculated and measured results.
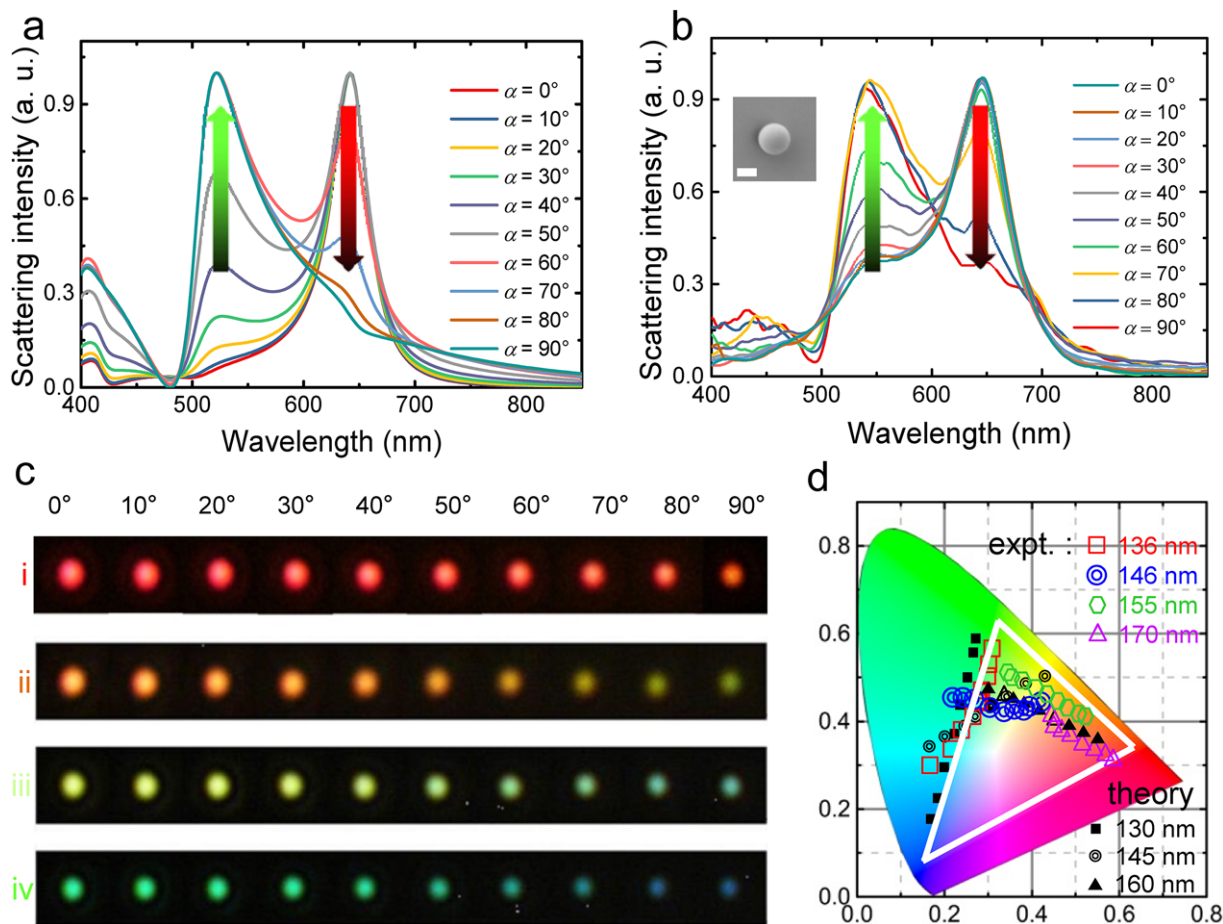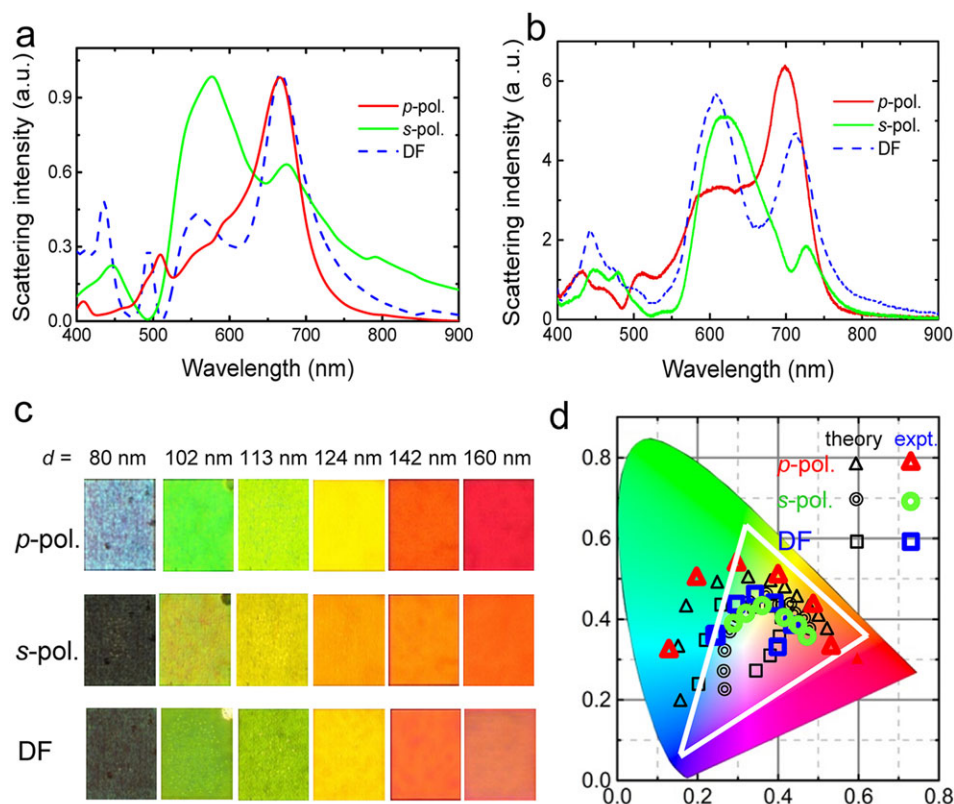
Figure 3. Tuning of the scattering light color by changing the polarization angle. Evolution of forward scattering spectrum with increasing polarization angle a) calculated and b) measured for a Si NS with $d = 160$ nm. The SEM image of the Si NS is shown in the inset of (b). The length of the scale bar is 100 nm. c) Evolution of the scattering light color with increasing polarization angle of the incident light measured for four Si NSs with different diameters. d) Color indices of the scattering light calculated (theory) and measured (expt.) for Si NSs with different diameters at different polarization angles from 10° to 90°.

In Figure 3c, we present the evolution of the scattering light with increasing polarization angle at an interval of 10° measured for four typical Si NSs with different diameters. When the polarization angle is increased from 0° to 90°, it can be seen that the scattering light is changed from red to pink for the largest Si NS with $d = 170$ nm (the first row). For the second largest Si NS with $d = 155$ nm (the second row), it evolves from orange to green. The scattering light of the moderate Si NS with $d = 146$ nm (the third row) is changed from yellow to sky-blue while that for the smallest Si NS with $d = 136$ nm (the fourth row) is changed from green to blue. For Si NSs with different diameters, we have simulated their scattering spectra by using the theoretical model based on Equation (6) and (7) and derived the corresponding color indices, as shown in Figure 3d by black symbols. The derivation of the color indices from the scattering spectra are described in detail in section 6 of Supplementary. The three vertices of the white triangle represent standard RGB colors. It is noticed that the color index of the scattering light of a Si NS can be varied within a wide range by changing only the polarization angle, implying the possibility of tuning the scattering light color. It is also remarkable that the chromaticity of the scattering light is quite good because most color indices are close to the sides of RGB triangle. More importantly, nearly all the colors can be achieved by selecting Si NSs with different sizes and by varying the polarization angle. Since the polarization of the incident light can be easily controlled by using a spatial light modulator, the strong dependence of the scattering light color on the polarization suggests a simple way to realize color-tuning display with a spatial resolution close to the optical diffraction limit. In Figure 3d, we also show the dependence of the color index on the polarization angle derived for the four Si NSs from the measured scattering spectra by using color symbols. Qualitative agreement between the calculated results and the experimental data is observed. The small discrepancy originates mainly from the deviation of the incident angle from the critical angle, which introduces a finite phase difference between the incident and reflected light.

As mentioned above, the phase difference between the incident and reflected light depends strongly on the polarization angle and incidence angle. At the critical angle, the phase difference is zero. For p-polarized light, the scattering spectrum at the critical angle is dominated by the MD resonance. When the incidence angle is increased from the critical angle ($\theta = 43.5°$) to

ADVANCED
SCIENCE NEWS

www.advancedsciencenews.com

LASER
&PHOTONICS
REVIEWS

www.lpr-journal.org

Figure 4. Arrays of regularly arranged Si NPs exhibiting different scattering light colors. Normalized scattering spectra a) calculated and b) measured for a Si NP with $d = 160$ nm and $h = 130$ nm which is illuminated by using s-polarized, p-polarized and un-polarized light. c) Scattering light colors exhibited by regular arrays of Si NPs with different diameters and the same height ($h = 130$ nm) under different illumination schemes. DF represents dark-field microscopy. d) Color indices of the scattering light calculated and measured for Si NPs with different diameters under different illumination schemes.

90°, the intensity of the MD resonance decreases while that of the ED resonance increases. The situation is reversed for the s-polarized light (see Supplementary Figure S7). Therefore, one can also change the scattering light color by varying the incidence angle. In practice, however, changing the polarization angle is more convenient than changing the incidence angle. In addition, the scattering light color is more sensitive to the polarization angle and a larger variation of color index can be achieved by varying the polarization angle, as demonstrated above.
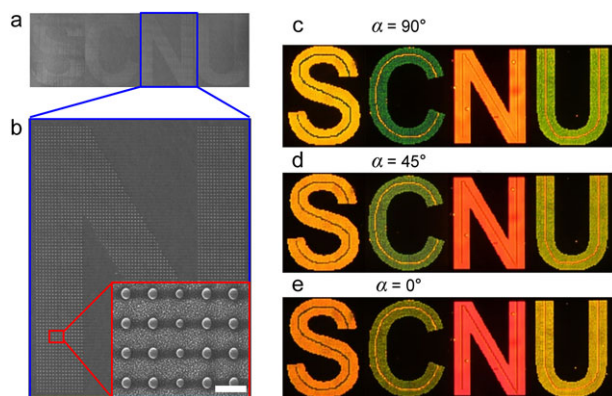
From the viewpoint of practical application in multicolor display with ultrahigh resolution, it is necessary to fabricate regular arrays of Si nanoparticles. Although it has been demonstrated that such kind of arrays can be realized by using laser printing technique,[55,56] the size uniformity and mechanical stability of the constituent Si NSs need to be improved for practical application. Therefore, it is highly desirable that Si NSs can be replaced by Si NPs which can be fabricated by using electron beam lithology and reactive ion etching, which are compatible with the current fabrication technology of Si chips.

Similar to Si NSs, Si NPs also exhibit distinct ED and MD resonances in their scattering spectra. Selective excitation of the ED or MD resonance of a Si NP can also be realized by using s- and p-polarized light and the change in the scattering light color can be achieved by varying the polarization angle. In **Figure 4**a, we show the forward scattering spectra calculated for a Si NP

with $d = 160$ nm and height of $h = 130$ nm excited by using s- and p-polarized light (see Supplementary Figs. S8 for the optimized height of Si NPs). The forward scattering spectrum obtained by using a plane wave under normal incidence is also provided for comparison. Similar to Si NSs, the selective excitation of the ED or MD resonance can also be achieved by using s- or p-polarized light, although the removal of the other component (ED or MD resonance) is not as complete as that observed in Si NSs (see Figure 3a).

In experiments, we have fabricated regular arrays of c-Si NPs on a silica substrate, which is a big challenge from the technological point of view (see Methods for the details). The forward scattering spectra measured for a single Si NP with $d = 162$ nm and $h = 130$ nm are shown in Figure 4b, which exhibit very good agreement with the calculated results shown in Figure 4a.

In Figure 4c, we show the scattering light colors exhibited by six regular arrays of Si NPs with different diameters. The arrays of Si NPs were illuminated by using p- (the first row) and s-polarized light (the second row) and un-polarized light in a dark-field microscope (the third row). Apart from the dependence of the scattering light color on the size of the constituent Si NPs, it is found that the scattering light color also depends strongly on the polarization angle of the incident light. In Figure 4d, we present the color indices derived for Si NP with diameters ranging from 80 to 190 nm and the same height of $h = 130$ nm, which

ADVANCED
SCIENCE NEWS

www.advancedsciencenews.com

LASER
& PHOTONICS
REVIEWS

www.lpr-journal.org

Figure 5. Arrays of regularly arranged Si NPs for color-tuning display. a) SEM image of the regularly-arranged Si NPs which form four letters of "SCNU". b) Magnified SEM image of letter "N". The inset shows some Si NPs with a further magnification. In each letter, the diameter of the Si NPs in the central curve is intentionally made to be different from the others. The length of the scale bar is 500 nm. c–e) CCD images of "SCNU" observed at different polarization angles showing the possibility of color-tuning display by simply varying the polarization angle of the illumination light.

are excited by using p-, s- and un-polarized light, respectively. As compared with Si NSs, the sensitivity of the scattering light color to the polarization angle is reduced to some extent. It is noticed that the color indices derived for the dark-field illumination are located at the center of the RGB triangle. In sharp contrast, it is found that most color indices derived for the excitation of p- and s-polarized light are located near the sides of the triangle, implying an improved chromaticity of the scattering light.

Figure 5a shows the SEM image of crystal-Si NPs with different diameters regularly arranged on square lattices with the same period (p) of 500 nm (see Supplementary Figure S10 for a larger period of 800 nm). They create four letters (i.e., "SCNU") which represent our university. The magnified SEM images of the letter "N" and the constitute Si NPs are shown in Figure 5b. From the top view of the Si NPs shown in the inset, it can be seen that the Si NPs possess circular cross section and uniform diameter. In addition, the Si NPs in the central line have a smaller diameter than that of the surrounding Si NPs, creating a defect line in each letter. In order to examine the spatial resolution, the diameter of the Si NPs that form the central curve is intentionally made to be different from that of the others. From the scattering light of the four letters under the illumination of evanescent wave, one can easily distinguish that the color of the central curve is different from that of the surrounding. In addition, we can see the obvious change in the scattering light color for each letter when the polarization angle is changed, as shown in Figure 5c–e. It demonstrates that a regular array of Si NPs, which is illuminated by an evanescent wave whose polarization is controlled by using a spatial light modulator, can be used to realize multicolor display. As compared with Si NSs (see Figure 3c), the scattering light color of Si NPs is not so sensitive to the polarization angle of the incident light (see Figure 5c–e). We think that the main reason is the deviation of the height of the fabricated Si NPs from the designed value of $\approx$130 nm, resulting in the broadening of the ED and MD resonances (see Supplementary Figure S11). In ad-

dition, the excitation efficiency is expected to decrease for Si NPs with height larger than 150 nm because the electric and magnetic fields decrease rapidly from the surface (see Supplementary Figure S3).

In the arrays of regularly arranged Si NPs, the scattering light color of a Si NP will be affected by the neighboring Si NPs if the period becomes close to the optical diffraction limit. In Figure 5, the scattering light color of the central curve in letter "S" was designed to be green for $\alpha = 90°$. However, it did not appear to be green because of the small period of the array ($p = 500$ nm). We have examined by numerical simulation the influence of the period on the scattering light color of the Si NPs in the central line, which is the situation shown in Figure 5. It was found that the influence of the surrounding Si NPs could be eliminated for a larger period of $p = 800$ nm (see Supplementary Figure S12). This conclusion was supported by the experimental observation performed for the arrays with $p = 800$ nm (see Supplementary Figure S10). It indicates that the spatial resolution of the multi-color display based on the regular arrays of Si NPs is $\approx$800 nm.

In our method, the employment of evanescent wave excitation significantly enhances the scattering light intensity and completely eliminates the background noise (see also Supplementary Figure S9 and S10). This unique feature enables the use of only a single Si NP in a pixel for color display, leading to a high spatial resolution which is close to the optical diffraction limit. In addition, the selective excitation of the MD or ED resonance reduces the linewidth of the scattering spectrum, dramatically improving the chromaticity of the scattering light. More importantly, the strong dependence of the scattering light on the polarization angle offers the opportunity for tuning the scattering light color. Therefore, the combination of these three characteristics makes it possible to realize multicolor display with high spatial resolution and good chromaticity.

4. Conclusions

In summary, we have proposed and demonstrated a new strategy for realizing multicolor display with high spatial resolution and good chromaticity by exciting Si nanoparticles with evanescent wave and varying the polarization angle. The physical mechanism for color control relies on the manipulation of the orientations of the EDs and MDs induced in Si nanoparticles in the two beam illumination scheme. The ED or MD resonance of a Si NS in the forward scattering spectrum be independently excited by using s- and p-polarized light, leading to vivid structural color with enhanced scattering intensity (by more than two times) and suppressed background noise. The proposed multicolor display has been implemented on regular arrays of Si NPs, which are compatible with the current fabrication technology of Si chips. Our findings pave the way for realizing all-optical displayers with high spatial resolution and good chromaticity.

Supporting Information

Supporting Information is available from the Wiley Online Library or from the author.

[1] A. Kristensen, J. K. W. Yang, S. I. Bozhevolnyi, S. Link, P. Nordlander, N. J. Halas, N. A. Mortensen, *Nat. Rev. Mater.* **2017**, *2*, 16088

[2] Y. Gu, L. Zhang, J. K. W. Yang, S. P. Yeo, C.-W. Qiu, *Nanoscale* **2015**, *7*, 6409.

[3] X. Zhu, C. Vannahme, E. Hojlund-Nielsen, N. A. Mortensen, A. Kristensen, *Nat. Nanotechnol.* **2016**, *11*, 325.

[4] J.-M. Guay, A. Calà Lesina, G. Côté, M. Charron, D. Poitras, L. Ramunno, P. Berini, A. Weck, *Nat. Commun.* **2017**, *8*, 16095

[5] J. Olson, A. Manjavacas, L. Liu, W. S. Chang, B. Foerster, N. S. King, M. W. Knight, P. Nordlander, N. J. Halas, S. Link, *Proc. Natl. Acad. Sci. USA* **2014**, *111*, 14348.

[6] H. Wang, X. Wang, C. Yan, H. Zhao, J. Zhang, C. Santschi, O. J. F. Martin, *ACS Nano* **2017**, *11*, 4419.

[7] X. M. Goh, Y. Zheng, S. J. Tan, L. Zhang, K. Kumar, C. W. Qiu, J. K. Yang, *Nat. Commun.* **2014**, *5*, 5361.

[8] M. Miyata, H. Hatada, J. Takahara, *Nano Lett.* **2016**, *16*, 3166.

[9] L. Duempelmann, D. Casari, A. Luu-Dinh, B. Gallinet, L. Novotny, *ACS Nano* **2015**, *9*, 12383.

[10] F. Cheng, J. Gao, L. Stan, D. Rosenmann, D. Czaplewski, X. Yang, *Opt. Express* **2015**, *23*, 14552.

[11] A. S. Roberts, A. Pors, O. Albrektsen, S. I. Bozhevolnyi, *Nano Lett.* **2014**, *14*, 783.

[12] J. S. Clausen, E. Højlund-Nielsen, A. B. Christiansen, S. Yazdi, M. Grajower, H. Taha, U. Levy, A. Kristensen, N. A. Mortensen, *Nano Lett.* **2014**, *14*, 4499.

[13] T. D. James, P. Mulvaney, A. Roberts, *Nano Lett.* **2016**, *16*, 3817.

[14] M. L. Tseng, J. Yang, M. Semmlinger, C. Zhang, P. Nordlander, N. J. Halas, *Nano Lett.* **2017**, *17*, 6034.

[15] T. Chen, B. M. Reinhard, *Adv. Mater.* **2016**, *28*, 3522.

[16] G. J. Stec, A. Lauchner, Y. Cui, P. Nordlander, N. J. Halas, *ACS Nano* **2017**, *11*, 3254.

[17] Z. Li, W. Wang, D. Rosenmann, D. A. Czaplewski, X. Yang, J. Gao, *Opt. Express* **2016**, *24*, 20472.

[18] K. Kumar, H. Duan, R. S. Hegde, S. C. W. Koh, J. N. Wei, J. K. W. Yang, *Nat. Nanotechnol.* **2012**, *7*, 557.

[19] J. Olson, A. Manjavacas, T. Basu, D. Huang, A. E. Schlather, B. Zheng, N. J. Halas, P. Nordlander, S. Link, *ACS Nano* **2016**, *10*, 1108.

[20] D. G. Baranov, D. A. Zuev, S. I. Lepeshov, O. V. Kotov, A. E. Krasnok, A. B. Evlyukhin, B. N. Chichkov, *Optica* **2017**, *4*, 814.

[21] A. Garcia-Etxarri, R. Gomez-Medina, L. S. Froufe-Perez, C. Lopez, L. Chantada, F. Scheffold, J. Aizpurua, M. Nieto-Vesperinas, J. J. Saenz, *Opt. Express* **2011**, *19*, 4815.

[22] A. B. Evlyukhin, C. Reinhardt, A. Seidel, B. S. Lukyanchuk, B. N. Chichkov, *Phys. Rev. B* **2010**, *82*.

[23] A. B. Evlyukhin, S. M. Novikov, U. Zywietz, R. L. Eriksen, C. Reinhardt, S. I. Bozhevolnyi, B. N. Chichkov, *Nano Lett.* **2012**, *12*, 3749.

[24] Y. H. Fu, A. I. Kuznetsov, A. E. Miroshnichenko, Y. F. Yu, B. Luk'yanchuk, *Nat. Commun.* **2013**, *4*, 1527.

[25] I. Staude, A. E. Miroshnichenko, M. Decker, N. T. Fofang, S. Liu, E. Gonzales, J. Dominguez, T. S. Luk, D. N. Neshev, I. Brener, Y. Kivshar, *ACS Nano* **2013**, *7*, 7824.

[26] T. Feng, Y. Xu, W. Zhang, A. E. Miroshnichenko, *Phys. Rev. Lett.* **2017**, *118*, 173901.

[27] A. Krasnok, S. Lepeshov, A. Alú, arXiv preprint arXiv:1801.00698, **2018**.

[28] J. Proust, F. Bedu, B. Gallas, I. Ozerov, N. Bonod, *ACS Nano* **2016**, *10*, 7761.

[29] S. Sun, Z. Zhou, C. Zhang, Y. Gao, Z. Duan, S. Xiao, Q. Song, *ACS Nano* **2017**, *11*, 4445.

[30] D. Permyakov, I. S. Sinev, D. Markovich, Y. Kivshar, *Appl. Phys. Lett.* **2015**, *106*, 171110.

[31] V. Flauraud, M. Reyes, R. Paniagua-Domłnguez, A. I. Kuznetsov, J. Brugger, *ACS Photonics* **2017**, *4*, 1913.

[32] X. Fang, M. L. Tseng, D. P. Tsai, N. I. Zheludev, *Phys. Rev. Appl.* **2016**, *5*, 014010.

[33] M. L. Tseng, X. Fang, V. Savinov, P. C. Wu, J. Y. Ou, N. I. Zheludev, D. P. Tsai, *Sci. Rep.* **2017**, *7*, 44488.

[34] Z. Dong, J. Ho, Y. F. Yu, Y. H. Fu, R. Paniagua-Dominguez, S. Wang, A. I. Kuznetsov, J. K. W. Yang, *Nano Lett.* **2017**, *17*, 7620.

[35] L. Cao, P. Fan, E. S. Barnard, A. M. Brown, M. L. Brongersma, *Nano Lett.* **2010**, *10*, 2649.

[36] M. Khorasaninejad, N. Abedzadeh, J. Walia, S. Patchett, S. S. Saini, *Nano Lett.* **2012**, *12*, 4228.

[37] S. S. Mirshafieyan, J. Guo, *Opt. Express* **2014**, *22*, 31545.

[38] E. Hojlund-Nielsen, J. Weirich, J. Nørregaard, J. Garnæs, N. A. Mortensen, A. Kristensen, *J. Nanophotonics* **2014**, *8*, 083988.

[39] V. Vashistha, G. Vaidya, R. S. Hegde, M. Krawczyk, *ACS Photonics* **2017**, *4*, 1076.

[40] X. Zhu, W. Yan, U. Levy, N. A. Mortensen, A. Kristensen, *Sci. Adv.* **2017**, *3*, e1602487.

[41] A. E. Miroshnichenko, S. Flach, Y. S. Kivshar, *Rev. Mod. Phys.* **2010**, *82*, 2257.

[42] D. Franklin, Y. Chen, V.-A. Guardado, S. Modak, J. Boroumand, D. Xu, S. T. Wu, D. Chanda, *Nat. Commun.* **2015**, *6*, 7337.

[43] G. Wang, X. Chen, S. Liu, C. Wong, S. Chu, *ACS Nano* **2016**, *10*, 1788.

[44] Z. Li, A. W. Clark, J. M. Cooper, *ACS Nano* **2016**, *10*, 492.

[45] X. Duan, S. Kamin, N. Liu, *Nat. Commun.* **2017**, *8*, 14606.

[46] V. Vashistha, G. Vaidya, P. Gruszecki, A. E. Serebryannikov, M. Krawczyk, *Sci. Rep.* **2017**, *7*, 8092.

[47] J. M. Geffrin, B. García-Cámara, R. Gómez-Medina, P. Albella, L. S. Froufe-Pérez, C. Eyraud, A. Litman, R. Vaillon, F. González, M. Nieto-Vesperinas, J. J. Sáenz, F. Moreno, *Nat. Commun.* **2012**, *3*, 1171.

[48] H. Li, Y. Xu, J. Xiang, X. F. Li, C. Y. Zhang, S. L. Tie, S. Lan, *Nanoscale* **2016**, *8*, 18963.

[49] O. Brzobohaty, V. Karasek, M. Siler, L. Chvatal, T. Cizmar, P. Zemanek, *Nat. Photonics* **2013**, *7*, 123.

[50] J. Chen, J. Ng, Z. Lin, C. T. Chan, *Nat. Photonics* **2011**, *5*, 531.

[51] J. Xiang, J. Li, H. Li, C. Zhang, Q. Dai, S. Tie, S. Lan, *Opt. Express* **2016**, *24*, 11420.

[52] E. D. Palik, *Handbook of optical constants of solids*, Academic Press, **1998**.

[53] A. E. Miroshnichenko, A. B. Evlyukhin, Y. S. Kivshar, B. N. Chichkov, *ACS Photonics* **2015**, *2*, 1423.

[54] A. B. Evlyukhin, T. Fischer, C. Reinhardt, B. N. Chichkov, *Phys. Rev. B* **2016**, *94*, 205434.

[55] U. Zywietz, A. B. Evlyukhin, C. Reinhardt, B. N. Chichkov, *Nat. Commun.* **2014**, *5*, 3402.

[56] J. Xiang, S. Jiang, J. Chen, L. Sheng, *Nano Lett.* **2017**, *17*, 4853.